

Lead Shock Velocity and Curvature Variation Across The Cellular Detonation Instability

Scott I. Jackson and Mark Short
Shock and Detonation Physics Group, Los Alamos National Laboratory,
Los Alamos, NM 87544

1 Introduction

Cellular instabilities occur for self-sustained detonation propagation in gaseous explosives. They are driven by acoustic-strength shocks propagating normal to the detonation shock surface in a Mach stem configuration. Experimental observations indicate that periodic transverse wave interactions are necessary for unsupported detonation propagation [1]. The instability cycle starts when transverse wave collisions locally increase the flow temperature, overdriving the shock, shortening the reaction zone (RZ), and tightly coupling the chemical RZ to the shock. The lead shock strength decays as it propagates and the transverse waves move further apart, resulting in gradual decoupling of the RZ until subsequent transverse wave interactions locally reinvigorate the flow and start the cycle anew. Early efforts [2–5] characterized the cellular cycle by measuring variations in the lead shock velocity with distance along the cell centerline. New cells exhibited highly overdriven centerline shock velocities ($1.5 D_{CJ}$), relative to the Champan-Jouguet solution, that rapidly and monotonically decreased over the cell length (to near $0.6 D_{CJ}$) in similar fashion to decaying inert shock wave [4]. The dynamics of off-centerline wavefront regions were not quantitatively examined and no comparisons were drawn to prior condensed-phase explosive research that developed relations between detonation velocity and shock front curvature [6–8].

Recently, there has been interest in performing more detailed characterization of gaseous detonation wavefronts using concepts derived from Detonation Shock Dynamics (DSD) theory. DSD is a surface propagation concept that replaces the detonation shock and RZ with a surface that evolves according to a normal-velocity evolution law [9–11]. Analysis of detonation shocks with quasi-steady shape and small wavefront curvature κ (relative to the inverse of the detonation RZ length) have shown that the local normal detonation velocity D_n is constant to leading order, with the first correction being a function of shock curvature such that $D_n = f(\kappa)$. This function is referred to as the explosive's velocity–curvature or D_n – κ relation and is experimentally measured. Higher-order corrections can also account for time-dependent and transverse flow effects in condensed explosives with large reaction zones [12]. Significantly, the D_n – κ relationship an explosive provides insight into its sensitivity and detonation propagation characteristics. Figure 1 illustrates this trend for ideal, insensitive, and nonideal for steady high-explosive detonations. Increasingly nonideal detonations have spatially larger reaction zones, a greater depreciation of detonation velocity with wave curvature, support detonation over a more limited curvature span, and thus are more influenced by wave geometry and confinement.

Application of DSD to gaseous detonations introduces several complications due to detonation unsteadiness associated with the cellular instability: (1) The impedance mismatch of gaseous explosives in solid confiners does not allow for the substantial postshock flow divergence present in high explosive systems, and (2) local cellular pulsations introduce large local and temporal variations in D_n and κ that preclude the assumption of small curvature and quasi-steady flow. Nevertheless, prior work has used DSD approaches to examine the initiation and evolution of the cellular structure. Numerical and approximate analytic efforts have reproduced cellular dynamics [14], predicted the existence of a limiting critical κ after which the detonation contained no sonic point [14, 15], and inferred minimum initiation energies for gaseous explosives [16]. A more recent approach [17] induced global

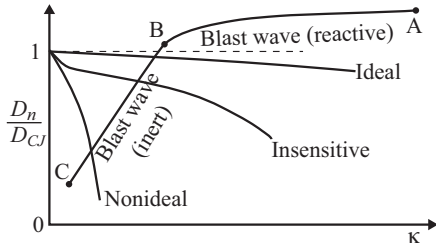


Fig. 1: $D_n-\kappa$ trends.

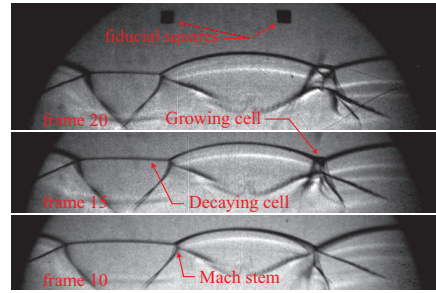


Fig. 2: Shadowgraph frames from NC260 [13].

wavefront curvature in excess of that produced by the cellular instability in order to establish a nondimensional $D_n-\kappa$ relationship for ethylene-oxygen mixtures. This approach was consistent with DSD’s intended purpose, which uses a surface propagation methodology to reduce the required computational effort (relative to direct numerical simulations using reactive flow models) to generate accurate wave shape and timing predictions while neglecting or homogenizing the smaller-scale details of the wave structure.

This study analyzes the evolution of weakly unstable cellular instabilities in $D_n-\kappa$ -space for both experimental and numerical detonation. We show that a classical leading-order DSD approach can not be used to model cellular dynamics due to the unsteady nature of the cellular decay, but that concepts from DSD provide insight into the time-dependent cellular mechanism and the relative sensitivity of gaseous explosive mixtures to geometric effects. In contrast to prior work, we focus on the $D_n-\kappa$ variation across the entire cellular front, rather than just the centerline.

2 Analysis of Narrow Channel Detonation

Variations in D_n and κ were derived from experiment using quasi-two-dimensional detonation shock shapes measured by Austin [13]. Her rectangular, narrow-channel (NC), detonation tube had a 152×18 mm cross section that damped out cellular instabilities across the 18-mm dimension (when the cell size $\lambda > 18$ mm), effectively approximating a two-dimensional cellular instability. We have analyzed successive shadowgraph frames (Fig. 2) of three separate experiments in two separate, weakly unstable, gaseous mixtures: $2H_2+O_2+17Ar$ (85% Ar by mole fraction, $D_{CJ} = 1.42$ mm/ μs , 0.20 bar, test # NC260) and $2H_2+O_2+12Ar$ (80%Ar by mole fraction, $D_{CJ} = 1.52$ mm/ μ , 0.20 bar, test # NC215 and NC229). As all gave similar results, only NC260 data is presented here.

An analytic equation with the functional form $z(x) = \ln(\cos(x))$, where z is the shock height and x is the transverse width, was first fit to each cell segment imaged and then differentiated to obtain D_n and κ . Successive front shapes fit in this fashion are shown in Fig. 3 for the 85%Ar mixture. Analytic fits (colored lines) are plotted over the black experimental data. The color of each analytic waveform corresponds to the phase ζ of each cell as shown in Fig. 4. Newly formed cells with ζ near 0 are violet; cells near the middle of their cycle ($\zeta \approx 0.5$) are green; and dying cells ($\zeta \rightarrow 1$) are red. The analytic fit correspondence to the experimental data is good overall.

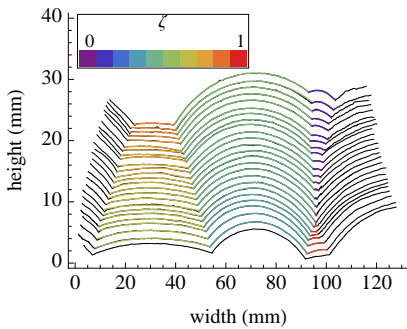


Fig. 3: Front points and fits for NC260.

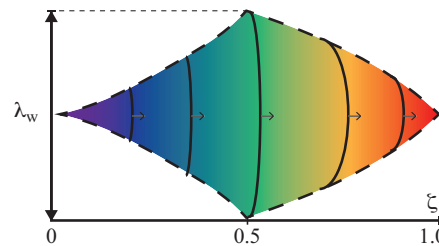
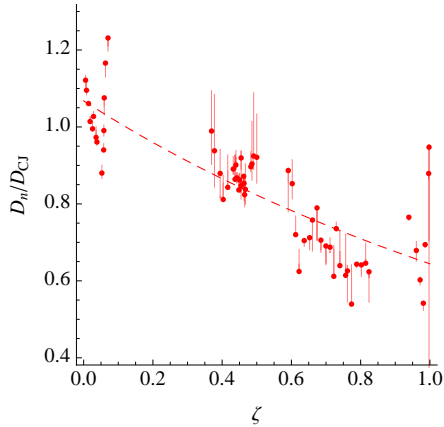
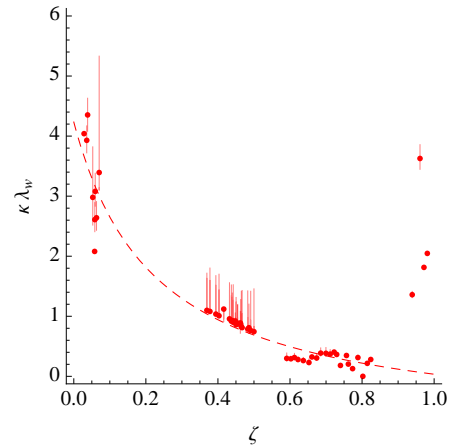


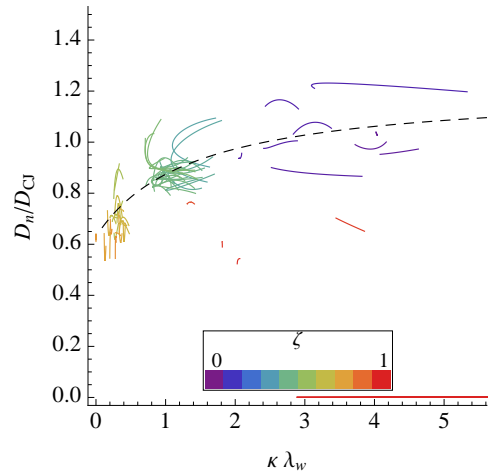
Fig. 4: A graphical description of ζ . Dashed lines denote triple point tracks; solid curves are the detonation shock at different timesteps.

Fig. 5: D_n variation with ζ for NC260.Fig. 6: κ variation with ζ for NC260.

The first-order fitting form used is not able to accurately capture the rapid variations in wavefront curvature near the edge of each cell, but these are explored further in the numerical work.

Local variations in D_n and κ across the front were then found from $D_n = D/(\sqrt{1 + (z')^2})$ and $\kappa = z''/[1 + (z')^2]^{3/2}$ where $z' = dz/dx$ and $z'' = d^2z/dx^2$. The above analysis is commonly performed with condensed explosive rate sticks which are designed to generate a steady detonation shape and axial velocity. The unsteady nature of the gaseous detonation front necessitated that local axial detonation velocity D be computed from the shock position shift between wavefront fits separated by four imaging timesteps: $D = (z_{(i+2)} - z_{(i-2)})/(4\tau)$. The limited observation time imposed by the framing camera record does not allow for substantial evolution of a single cell in the weakly unstable mixtures discussed, but permits simultaneous observation of multiple cells in different phases of evolution. Thus, separate experimental measurements are combined to study the full instability cycle with the assumption that all cells in a test generate a similar D_n and κ evolution across the front.

Figures 5 and 6 plot D_n and κ versus ζ . Each plot contains data points, solid lines, and a dashed line. The data points are the wavefront values along the cell centerline, as have been historically plotted in cellular studies [2–5]. Solid lines denote the span of D_n values (off of the cell centerline as) measured along each front profile. Dashed lines are least-squares fits to the cell centerline points using a $1/\zeta$ -functional form that is consistent with previous [2–5] experimental observations. Such a form is also consistent with that of an inert cylindrically expanding blast wave which can be shown to have a linear profile (Fig. 1, line BC) in velocity-curvature space, with $U_s = \frac{\alpha(\gamma)}{2} \sqrt{\frac{E_s}{\rho_0}} \frac{1}{r}$ where $\kappa = 1/r$. Figures 5 and 6 demonstrate that, at the cell centerline, the local shock velocity and curvature monotonically decrease throughout the cellular cycle. The range of wavefront curvature present away from the centerline axis is significantly larger for expanding cells as compared to shrinking ones. From this measurement, it is inferred that most curvature variation in a detonation cell occurs downstream of the Mach stem and that shrinking detonation cells assume an approximately cylindrical wavefront profile.

Fig. 7: D_n - κ variation for NC260.

Figures 5 and 6 can be combined to show the experimental D_n and κ evolution throughout the full cycle. Figure 7 plots this relationship versus ζ for the 85%Ar mixture. Solid lines correspond to the D_n - κ profiles for each cell segment, with ζ denoted by color. The dashed black line corresponds to the functional-form fits. The compiled measurements form a global trend with cells moving from the upper right of the plot to the lower left as the cell evolves. Early in the cellular cycle (small ζ), a wide range of κ variation is present over a small span of D_n . This low-slope D_n - κ trend indicates overdriven cell expansion

supported by a spatially narrow reaction zone, similar to D_n - κ trends observed for ideal high explosives (Fig. 1). Late in the cellular cycle (large ζ), the wave's D_n (κ) slope is significantly steeper; small changes in κ result in large D_n variations, which are consistent with non-ideal high explosive behavior (spatially long reaction zone, Fig. 1). Intermediate values of ζ show a gradual transition between these two limiting behaviors. Late-stage (red) cells exhibit excursions from this trend due to fitting inaccuracy in κ -space.

3 Numerical Simulation

High-resolution direct numerical simulation was also used to study the cellular wavefront evolution. Computations used a non-dimensional reactive Euler equation model assuming an ideal gas and one-step Arrhenius-type reaction with a shock-fit, shock-attached solution method [18, 19] that allowed straightforward determination of the lead shock κ and D_n . Numerical parameters were fit [20] to the 80%Ar mixture using the $2H_2$ - O_2 -Ar kinetic

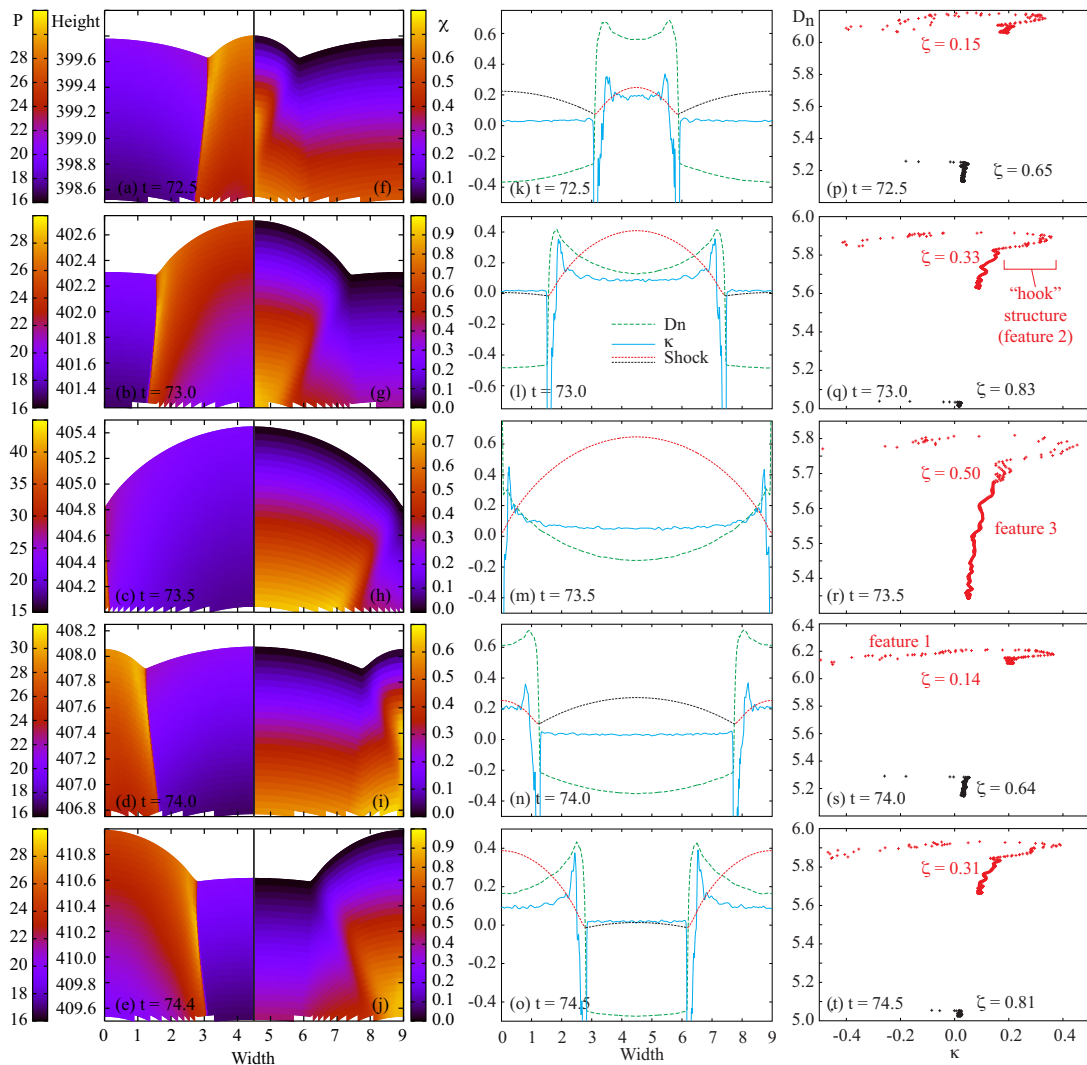


Fig. 8: Computed instantaneous pressure profiles (a)–(e); RZ progress (f)–(j); D_n (green, long-dashed), κ (blue, solid), and shock height (black or red, short-dashed) versus width (k)–(o); and D_n - κ (p)–(t) profiles for five timesteps of the 80% Ar computation. For (k)–(o), plotted D_n values are relative to 5.5, while shock loci have been displaced by (k) -399.5 , (l) -402.3 , (m) -404.8 , (n) -407.8 and (o) -410.6 . Plots (p)–(t) show the D_n - κ variation for each corresponding shock segment from plots (k)–(o).

mechanism of Ref. [21] yielding $E = \tilde{E}/\tilde{R}\tilde{T}_0 = 20$, $Q = \tilde{Q}/\tilde{R}\tilde{T}_0 = 10$ and $\gamma = 1.57$. Length was scaled with $\tilde{l}_{1/2}=0.72$ mm, the distance between the shock and the point where half of the reactant is depleted in the ZND wave, while time was scaled with $\tilde{l}_{1/2}/\sqrt{\tilde{p}_0/\tilde{\rho}_0}=2.68$ μs . Consequently, the non-dimensional reaction rate constant $k = 22.719$ and $D_{CJ} = 5.517$. Resolution requirements limited the 2-D channel of width to 9 (dimensionally 9 times $\tilde{l}_{1/2}$), which was smaller than the experimental channel size. The computational zone length was 40, with the lead shock located at $x = 0$ and an outflow boundary at $x = -40$. Axial and transverse resolutions were 0.05 (corresponding to 20 points per half reaction length) and 0.0125 (80 points per half reaction length), respectively. The initial conditions consisted of a 1-D ZND structure with a two-dimensional mass fraction perturbation to generate the cellular instability.

The calculation both confirms the experimental observations and characterizes the lead shock velocity and curvature variations in unprecedented detail. Figure 8 shows snapshots of the cellular pressure profile (a)–(e), reaction progress variable (f)–(j) in the vicinity of the shock front, D_n and κ spatial variation (k)–(o) across the shock, and the corresponding instantaneous D_n – κ map (p)–(t) for multiple timesteps though out the cellular cycle. Red and black data indicate growing and decaying cells, respectively, for the shock loci data in Fig. 8 (k)–(o) and the D_n – κ map in Fig. 8 (p)–(t).

Growing cells exhibit the highest velocity and curvature spans in the portion of the growing cell just downstream of the Mach stem (Fig.8 (k)–(o)). Curvature first extends to negative values (concave facing the direction of bulk wave motion) immediately adjacent to Mach stem before peaking a short distance away towards the cell center-line. Further towards the cell center, the shock exhibits monotonically decreasing local velocity and curvature. Decaying cells exhibit significantly less variation in D_n and κ . In velocity–curvature space (Fig. 8 (p)–(t)), these behaviors map to three distinct features: (feature 1) a low slope, large-curvature-span flat curve for the reactive flow immediately adjacent to the Mach stem, which is characteristically similar to the velocity–curvature profile of an ideal explosive with a spatially small reaction zone (*cf. Fig.1, ideal*); (feature 2) a “hook” structure associated with the peak velocity and curvature values followed by partial RZ decoupling (*cf. Fig.1, line AB*); and (feature 3) a high-slope, narrow-curvature-span flat curve characteristic of both a highly nonideal explosive (*cf. Fig.1, nonideal*), which only supports detonation over a narrow curvature range relative to ideal explosives, and an inert cylindrical decaying blast wave, which has a linear trajectory in velocity–curvature space (*cf. Fig.1, line BC*).

Comparison of cells in different stages of evolution (Fig. 9) shows that, in velocity–curvature space, all low-slope (feature 1) and hook (feature 2) profiles occur above the Chapman–Jouguet velocity, but do not overlay. Below the Chapman–Jouguet velocity, all high-slope curves (feature 3) overlay well. Newly developed, growing cells only display features 1 and 2. As the growing cells evolved, feature 3 first appeared and subsequently grew in span. As the cell begin to shrink due to encroachment of Mach stems from neighboring cells, features 1 and 2 are eliminated from the velocity–curvature profile, leaving only feature 3. The curvature span of feature 3 decreases with the size of the decaying cell. The low-slope (feature 1) and hook (feature 2) structures are associated with high and decreasing levels of reaction zone strength and shock coupling. The high-slope (feature 3) region is attributed to an inert expanding cylindrical shock wave. The data indicates that, for weakly unstable detonation, coupling between the shock and reaction zone only occurs near the Mach stem in growing cells and that the lead shock diffracts in an inert fashion away from this region. Exceeding the Chapman–Jouguet velocity appeared to be a necessary condition for shock and reaction zone coupling to exist in the single computation presented.

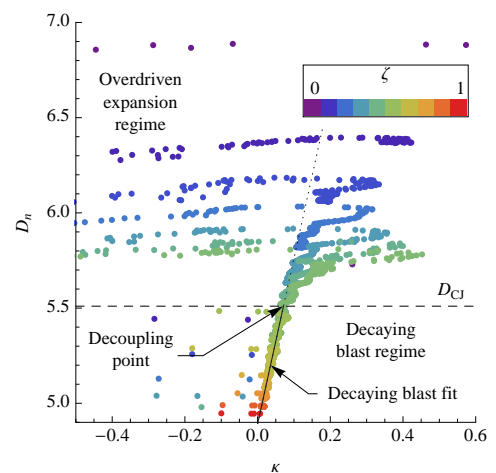


Fig. 9: Numeric D_n – κ variation with ζ .

References

- [1] M. Radulescu and J. Lee, “The failure mechanism of gaseous detonations: Experiments in porous wall tubes,” *Combustion and Flame*, vol. 131, pp. 29–46, 2003.

- [2] R. Strehlow and A. Crooker, “The structure of marginal detonation waves,” *Acta Astronautica*, vol. 1, pp. 303–315, 1974.
- [3] D. Edwards and A. Jones, “The variation in strength of transverse shocks in detonation waves,” *J. Phys. D: Appl. Phys.*, vol. 11, pp. 155–166, 1978.
- [4] E. A. Lundstrom and A. K. Oppenheim, “On the influence of non-steadiness on the thickness of the detonation wave,” *Proc. R. Soc. A*, vol. 310, no. 1503, pp. 463–478, 1969.
- [5] M. Dormal, J.-C. Libuton, and P. V. Tiggelen, “Evolution of induction time in detonation cells,” *Acta Astronautica*, vol. 6, pp. 875–884, 1979.
- [6] H. Jones, “A theory of the dependence of the rate of detonation of solid explosives on the diameter of the charge,” *Proc. Royal Soc., Series A*, vol. 1018, pp. 415–426, 1947.
- [7] H. Eyring, R. P. G. Duffey, and R. Parlin, “The stability of detonation,” *Chem. Rev.*, vol. 45, pp. 69–181, 1949.
- [8] W. Wood and J. Kirkwood, “Diameter effect in condensed explosives. the relation between velocity and radius of curvature of the detonation wave,” *Journal of Chemical Physics*, vol. 22, no. 11, pp. 1920–1924, 1954.
- [9] J. Bdzil, “Steady-state two-dimensional detonation,” *Journal of Fluid Mechanics*, vol. 108, pp. 195–226, 1981.
- [10] J. B. Bdzil, W. Fickett, and D. S. Stewart, “Detonation shock dynamics: A new approach to modeling multi-dimensional detonation waves,” in *Ninth Symposium (Int.) on Detonation*, pp. 730–742, Office of Naval Research, 1989.
- [11] J. Bdzil and D. Stewart, “The dynamics of detonation in explosive systems,” *Ann. Rev. Fluid Mech.*, vol. 39, pp. 263–292, 2007.
- [12] J. Bdzil, T. Aslam, and M. Short, “DSD front models: Nonideal explosive detonation in ANFO,” in *Twelfth Symposium (Int.) on Detonation*, pp. 409–417, 2002.
- [13] J. Austin, *The Role of Instability in Gaseous Detonation*. PhD thesis, California Institute of Technology, 2003.
- [14] J. Yao and D. Stewart, “On the normal detonation shock velocity–curvature relationship for materials with large activation energy,” *Combustion and Flame*, vol. 100, pp. 519–528, 1995.
- [15] R. Klein, J. Krok, and J. Shepherd, “Curved quasi-steady detonations: Asymptotic analysis and detailed chemical kinetics,” Tech. Rep. FM95-04, Graduate Aeronautical Laboratories, California Institute of Technology, Pasadena, CA, February 1996.
- [16] L. He and P. Calvin, “On the direct initiation of gaseous detonations by an energy source,” *Journal of Fluid Mechanics*, vol. 277, pp. 227–248, 1994.
- [17] H. Nakayama, T. Moriya, J. Kasahara, A. Matsuo, Y. Sasamoto, and I. Funaki, “Stable detonation wave propagation in rectangular-cross-section curved channels,” *Combustion and Flame*, vol. 159, 2011.
- [18] A. Henrick, T. Aslam, and J. Powers, “Simulations of pulsating one-dimensional detonations with true fifth order accuracy,” *J. Computat. Phys.*, vol. 213, pp. 311–329, 2006.
- [19] A. Henrick, *Shock-fitted numerical solutions of one- and two-dimensional detonation*. PhD thesis, University of Notre Dame, 2008.
- [20] S. Lau-Chapdelaine and M. Radulescu. personal communication, 2012.
- [21] J. Li, Z. Zhao, A. Kazakov, and F. L. Dryer, “An updated comprehensive kinetic model of hydrogen combustion,” *Int. J. Chem. Kinet.*, vol. 36, pp. 566–574, 2004.